Engineering Analysis with Boundary Elements 87 (2018) 19–26

Contents lists available at ScienceDirect

Engineering Analysis with Boundary Elements

journal homepage: www.elsevier.com/locate/enganabound

Continuous–discontinuous hybrid boundary node method for frictional contact problems

Bing-Di Zhong[a], Fei Yan[b,*], Jia-He Lv[b]

[a] School of Automobile and Traffic Engineering, Wuhan University of Science and Technology, Wuhan 430081, China
[b] State Key Laboratory of Geomechanics and Geotechnical Engineering, Institute of Rock and Soil Mechanics, Chinese Academy of Sciences, Wuhan 430071, China

ARTICLE INFO

Keywords:
Meshless method
Hybrid boundary node method
Frictional contact problem
Continuous–discontinuous hybrid boundary node method
Discontinuous interpolation

ABSTRACT

This paper presents a continuous–discontinuous hybrid boundary node method for frictional contact problems. In this method, the outer and internal boundaries are divided into several individual segments, for a continuous segment on outer boundary, the radial point interpolation method (RPIM) is employed for shape function construction, for discontinuous segments, the enriched discontinuous basis functions combined with RPIM are developed, in order to reflect the local field property of displacement and stress around crack tip, different basis functions for displacement and traction are developed for shape function construction on discontinuous segments individually. And the near tip asymptotic field functions and Heaviside function are employed for simulating the high gradient of stress field and discontinuous displacement field on contact surfaces. Besides a frictional contact theory and complementation detail for the present method is proposed, and some additional equations are developed for frictional contact iteration. Based on above technique and theory, a continuous–discontinuous hybrid boundary node method is proposed for frictional contact problems. Some numerical examples are shown that the present method is effective and can be widely used for some frictional contact engineering.

1. Introduction

The frictional contact problems are one of the most important problems in civil, mechanical and engineering areas. At the same time, it is also one of the most difficult problems to simulate by numerical method, because they are always nonlinear, and the convergence of frictional iteration is always difficult, besides, many geometric and mathematical models are also difficult to choose. Then it is a challenging task to model and simulate a frictional contact problem, such as sheet metal forming, cam mechanism rotating, bridge bearing, impact and penetration. Those types of problems can be modeled with adaptive finite element method (FEM) method using the penalty method [1–2] and variational inequalities [3], but high-level mesh density must be enforced around contact region. Hughes et al. [4] proposed a finite element analysis method for contact problem with a small deformation assumption.

Besides widely used of FEM for frictional contact problems, boundary element method (BEM) is also employed for simulating frictional contact problem, such as, Xiao and Yue [5] proposed a generalized Kelvin solution based BEM for contact problems of elastic indenter on functionally graded materials, and Gun and Gao [6] proposed a quadratic BEM formulation for continuous non-homogeneous, isotropic and linear elastic functionally graded material contact problems with friction. Olukoko et al. [7] gave a review of three alternative approaches to modeling frictional contact problems using the boundary element method. Hack and Becker [8] developed a local axes boundary element formulation for analysis of frictional contact problems under tangential loading. Gun [9] used boundary element method to simulate 3D elasto-plastic contact problems with friction.

Many meshless methods have been proposed in literature for analysis frictional contact problems. Aimed to overcome contact constraints and solving contact problems, an adaptive meshless method (MLM) for solving mechanical contact problems is proposed by Li and Lee [10], which automatically insert additional nodes into large error regions identified in terms of mechanical stresses, and it is a combination of a sliding line algorithm and the penalty method, thus, it can solve nonlinear contact problems with large deformation. Belaasilia et al. [11] applied a numerical mesh-free model for simulating elasto-plastic structures with contact, which is based on the asymptotic numerical method and it is in the meshless collocation framework. Gun [12] presented a quadratic meshless boundary element formulation for isotropic damage analysis of contact problems with friction.

As a widely used meshless method, the meshless local Petrov–Galerkin (MLPG) approach for large deformation contact analysis is developed by Hu et al. [13], in which the MLPG approach was based on a local weak form with RBF coupled with polynomial basis function. Xiao

* Corresponding author.
E-mail address: fyan@whrsm.ac.cn (F. Yan).

https://doi.org/10.1016/j.enganabound.2017.11.007
Received 11 October 2017; Accepted 15 November 2017
Available online 23 November 2017
0955-7997/

et al. [14] combined subdomain variational inequality, MLPG method and radial basis functions for solving two-dimensional contact problems, which is based on the Heaviside step function and radial basis functions.

A new complex variable element free Galerkin (EFG) was investigated by Li et al. [15], in which the technique based on Galerkin weak form and the penalty method was used to impose essential boundary conditions. Timesli et al. [16,17] proposed a new algorithm on moving least square method to simulate material mixing in friction stir welding, and furthermore, Mesmoudi et al. [18] developed a 2D mechanical-thermal coupled model to simulate material mixing observed in friction stir welding process. Belytschko and Fleming [19] proposed a contact algorithm based on the penalty method combined with EFG method for contact problems. Tiago and Pimenta [20] implemented element free Galerkin with moving least square (MLS) to nonlinear analysis of plates undergoing arbitrary large deformations. Ullah and Augarde [21] developed an adaptive meshless approach based on EFG method for nonlinear solid mechanics. EFG was applied in the simulation of forging process by Guedes and Cesarde Sa [22], in which blending finite elements with EFG in order to overcome the difficulty of meshless methods in dealing with essential boundary conditions.

Besides, Youssef et al. [23] proposed a numerical mesh-free model for simulating elasto-plastic structures with contact, which was based on the asymptotic numerical method. Chen et al. [24] discussed some recent enhancements in meshfree methods for incompressible boundary value problems, in which a mixed transformation method and a boundary singular kernel method were applied for imposition of essential boundary condition and contact constraints. Campbell et al. [25] proposed a contact algorithm for smoothed particle hydrodynamics (SPH), Attaway et al. [26] coupled SPH and finite elements for a contact problem, Kulasegaram et al. [27] proposed a new approach to handle the contact between Lagrangian SPH particles and rigid solid boundaries. Kim et al. [28] used a meshless method for a frictional contact problem with a rigid body, in which a continuum-based shape design sensitivity formulation was proposed. Chen et al. [29] used a meshless method based on the reproducing kernel particle method (RKPM) for metal forming analysis. Li et al. [30,31] employed radial point interpolation method for contact analysis of solids and metal forming process. The boundary singular kernel method was proposed by Chen and Wang [32] for computation of contact problems.

Hybrid boundary node method (HBNM) [33] is derived from boundary node method, which is first proposed by Mukherjee [34], short after that, singular hybrid boundary node method is proposed by Miao et al. [35]. Later, Yan et al. employed dual reciprocity method (DRM) [36] to HBNM, and proposed the dual reciprocity hybrid boundary node method (DHBNM) to solve inhomogeneous [37], dynamic [38], nonlinear [39], and convection-diffusion problems [40] etc. furthermore, based on Shepard interpolation method and Taylor expansion, Yan et al. [41] propose a new shape function constructing method, i.e., the Shepard and Taylor interpolation method (STIM), and develop a continuous–discontinuous hybrid boundary node method [42] for crack propagation.

In this paper, a continuous–discontinuous hybrid boundary node method for frictional contact problems is presented, in which the outer and internal boundaries are divided into several individual segments, for continuous segments on outer boundary, the radial point interpolation method (RPIM) is employed for shape function construction, for discontinuous segments, the enriched discontinuous basis functions combined with RPIM are developed, and different basis functions are employed to construct shape functions for displacement and traction respectively to reflect the local field property of displacement and stress around crack tip. And the near tip asymptotic field functions and Heaviside function are employed for simulating the high gradient of stress field and discontinuous displacement field on contact surfaces. Besides a frictional contact theory and complementation detail for the present method is proposed, and some additional equations are developed for frictional contact iteration. Based on above technique and theory, a continuous–discontinuous hybrid boundary node method is proposed for frictional contact problems. Some numerical examples are shown that the present method is effective and can be widely used for some frictional contact engineering.

2. Continuous–discontinuous hybrid boundary node method

Consider a calculating domain Ω, and its boundary is Γ. According to theory of hybrid boundary node method, only boundary needs to be discrete, and the boundary is divided into several continuous segments in this method, and the variable interpolation is approximated on each continuous segment individually, then the shape function on continuous segment is constructed by radial point interpolation method, and discontinuity is approximated by the enriched discontinuous interpolation.

2.1. Continuous interpolation

Radial point interpolation method is employed in this section to construct shape function for the common continuous segments, by which the shape function has the delta function property, and boundary conditions can be applied easily and directly, and computational expense can be greatly reduced compared to moving least square.

According to theory of RPIM, the variables of displacement u on a continuous segment can be expressed as [43]

$$u(s) \approx u^h(s) = \sum_{i=1}^{N_S} R_i(r)a_i + \sum_{j=1}^{m} P_j(s)b_j \tag{1}$$

where N_S is the node number on approximating segment, s denotes parameter coordinate of approximating segment; and m ($m < N_S$) is the number of monomials basis, and the monomials basis is $P_j(s) = s^k \quad k = 0, 1, ..., m$; a_i, b_j are approximating coefficient; $R_i(r)$ is the RBF, for example: multi-quadrics (MQ) $R_i(r) = (r_i^2 + c^2)^q$; Gaussian (EXP) $R_i(r) = \exp[-br_i^2]$; thin plate spline (TPS) $R_i(r) = r_i^n \ln(r_i)$.

In order to obtain the constants coefficient a_i and b_j, Eq. (1) is enforced to be satisfied at N_S nodes at approximating segment, and combined with a constraint of the monomial basis and constant coefficient a_i, one get the system equations as follows [43]:

$$\tilde{\mathbf{u}}_0 = \begin{Bmatrix} \mathbf{u}_0 \\ 0 \end{Bmatrix} = \begin{bmatrix} \mathbf{R}_0 & \mathbf{P}_0 \\ \mathbf{P}_0^T & \mathbf{0} \end{bmatrix} \begin{Bmatrix} \mathbf{a} \\ \mathbf{b} \end{Bmatrix} = \mathbf{G}\mathbf{a}_0 \tag{2}$$

where $\mathbf{a}_0^T = [a_1, a_2, ..., a_{N_S}, b_1, b_2 ... b_m]$, $\mathbf{u}_0^T = [u(s_1), u(s_2), ..., u(s_{N_S}), 0, 0, 0]$, and $\mathbf{R}_0$ is the matrix of RBF values on each approximating nodes, $\mathbf{P}_0$ is the matrix of the monomials basis values on each approximating nodes.

Solving Eq. (2), one can get the approximating coefficients, which is

$$\mathbf{a}_0 = \mathbf{G}^{-1}\tilde{\mathbf{u}}_0 \tag{3}$$

Substituting Eq. (3) into Eq. (1), one can get the shape function of the present method, which can be given as

$$\mathbf{\Phi}^T(\mathbf{s}) = [\Phi_1(s), \Phi_2(s), ..., \Phi_{N_S}(s), ..., \Phi_{N_S+m}(s)] = [\mathbf{R}^T(\mathbf{r}) \quad \mathbf{P}^T(\mathbf{s})]\mathbf{G}^{-1} \tag{4}$$

So variables for the displacement on the common continuous boundary can be obtained as [43]

$$\tilde{\mathbf{u}}(\mathbf{s}) = \mathbf{\Phi}^T(\mathbf{s})\mathbf{u} = \begin{Bmatrix} \tilde{u}(s_1) \\ \tilde{u}(s_2) \\ \vdots \\ \tilde{u}(s_{N_S}) \end{Bmatrix} = \begin{Bmatrix} \sum_{i=1}^{N_S} \Phi_i(s_1)u_i \\ \sum_{i=1}^{N_S} \Phi_i(s_2)u_i \\ \vdots \\ \sum_{i=1}^{N_S} \Phi_i(s_{N_S})u_i \end{Bmatrix} \tag{5}$$

in which $\mathbf{u}^T = [u_1, u_2, ..., u_{N_S}]$. The same as Eq. (5), variables for the boundary traction can also be approximated by this shape function, which is

$$\tilde{\mathbf{t}}(\mathbf{s}) = \mathbf{\Phi}^T(\mathbf{s})\mathbf{t} \tag{6}$$

in which $\mathbf{t}^T = [t_1, t_2, ..., t_{N_S}]$ are nodal values on approximating nodes on continuous segment.

2.2. The enriched discontinuous interpolation

As we know, a discontinuous segment consists with the upper surface and the bottom surface, and the displacements on the upper and bottom surfaces may different, which causes the discontinuous properties of stress. An enriched discontinuous interpolation is employed in this method to simulate the discontinuous displacement and stress of discontinuous structures, besides, the exact near-tip asymptotic field functions are used to simulate the high gradient stresses near crack tip.

Based on linear elastic fracture mechanics, the displacement around crack tip is a function of $r^{1/2}$, in which r is a polar coordinate in local crack tip coordinate system, then the radial basis function in Eq. (1) for discontinuous cracks can be given as [42]

$$\mathbf{p}^{\mathbf{T}}(\mathbf{s}) = [1, s, s^2, r^{1/2}] \tag{7}$$

Substituting Eq. (7) into Eq. (2), one can get the continuous part of shape function for displacement on discontinuous crack, which is

$$\tilde{u}(s) = \sum_{i=1}^{N_S} \Phi_i^u(s) u_i \tag{8}$$

in which $\Phi_i^u(s)$ is the continuous part of shape function related to Eq. (7). Compared to continuous structure, displacement and stress on discontinuous segment are discontinuous. Based on partition of unity, the shape function of displacement on discontinuous structure can be given as [42]

$$\tilde{u}(s) = \sum_{i=1}^{N_S} \Phi_i^u(s) u_i + \sum_{j=1}^{N_S} \Phi_j^u(s) H(\xi) \mathrm{a}_j \tag{9}$$

in which a_j is the additional degree of nodal freedom for modeling strong discontinuity, and the signed function is chosen as the Heaviside enrichment function, which is

$$H(\xi) = \begin{cases} 1 & \forall \xi \in \Gamma_s \\ -1 & \forall \xi \in \Gamma_t \end{cases} \tag{10}$$

in which ξ is distance from calculation node to crack surface, and $\xi > 0$ when calculation node is on upper of the crack surface, and $\xi < 0$ when calculation node is bottom of the crack surface, and $\xi = 0$ when the calculation nodes is located on the crack surface, which can be seen in Fig. 2.

In the present method, the displacement and traction on discontinuous segment and boundaries are approximated individually. The same as displacement approximating, the stress field around crack tip is a function of $r^{1/2}$, then the radial basis function in Eq. (1) for traction approximating on discontinuous cracks can be given as

$$\mathbf{p}^{\mathbf{T}}(\mathbf{s}) = \left[1, s, s^2, r^{-1/2}\right] \tag{11}$$

Substituting Eq. (11) into Eq. (2), one can get the continuous part of shape function for boundary traction, which is

$$\tilde{t}(s) = \sum_{i=1}^{N_S} \Phi_i^t(s) t_i \tag{12}$$

in which $\Phi_i^t(s)$ is the continuous part of shape function related to Eq. (11). The same as Eq. (9), the traction on discontinuous segment is discontinuous, then an enrichment shape function is constructed, which is

$$\tilde{t}(s) = \sum_{i=1}^{N_S} \Phi_i^t(s) t_i + \sum_{j=1}^{N_S} \Phi_j^t(s) H(\xi) \mathrm{b}_j \tag{13}$$

in which b_j is the additional degree of nodal freedom for modeling strong discontinuity of boundary tractions.

2.3. Hybrid boundary node method

Consider a 2D elasticity problem with domain Ω bounded by Γ. The governing equations are:

$$\sigma_{ij,j} = 0 \tag{14}$$

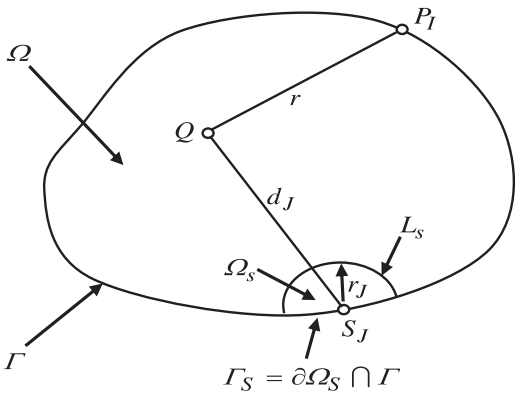

Fig. 1. Local domain and source point corresponding to s_J.

$$u_i = \hat{u}_i \quad \text{on } \Gamma_u \tag{15}$$

$$\sigma_{ij} n_j = \hat{t}_i \quad \text{on } \Gamma_t \tag{16}$$

where $\hat{u}_i$ and $\hat{t}_i$ denote boundary node values and n is the unit outward normal to the domain boundary Γ.

According to hybrid displacement variational theory, the total potential energy can be given as [33]

$$\Pi = \int_\Omega \frac{1}{2} u_{i,j} c_{ijkl} u_{kl} d\Omega - \int_\Omega \mathbf{u}^T \mathbf{b} d\Omega - \int_{\Gamma_t} \mathbf{u}^T \hat{\mathbf{t}} d\Gamma \tag{17}$$

where $\mathbf{u}$ is the displacement vector, $\hat{\mathbf{t}}$ is the boundary traction vector, and the coefficients $c_{ijkl} = \frac{2G\nu}{1-2\nu}\delta_{ij}\delta_{kl} + G\delta_{il}\delta_{jk}$, and G is the shear modulus.

Based on hybrid displacement variational principle and hybrid boundary node method [42,43], test function $h_J(Q)$ is used to replace the variational part, one can get

$$\int_{\Gamma_S + L_S} (t_i - \tilde{t}_i) h_J(Q) d\Gamma - \int_{\Omega_S} \sigma_{ij,j} h_J(Q) d\Omega = 0 \tag{18}$$

$$\int_{\Gamma_S + L_S} (u_i - \tilde{u}_i) h_J(Q) d\Gamma = 0 \tag{19}$$

in which the sub-domain Ω_s is chosen as the intersection of the domain Ω and a circle centered at a boundary node, s_J (Fig. 1) and the radius of the circle is r_J.

And test function $h_J(Q)$ is chosen to ensure that the integral about variable of $\tilde{u}_i$ and $\tilde{t}_i$ on L_s is equal to zero, then test function can be written as [42,43]

$$h_J(Q) = \begin{cases} \dfrac{\exp[-(d_J/c_J)^2] - \exp[-(r_J/c_J)^2]}{1 - \exp[-(r_J/c_J)^2]} & 0 \le d_J < r_J \\ 0 & d_J \ge r_J \end{cases} \tag{20}$$

where d_J is the distance between the integral point, Q, in the domain and the nodal point, s_J. c_J is a constant controlling the test function shape, r_J is the radius of the sub-domain.

Then Eqs. (18) and (19) can be rewritten as follows [42,43]:

$$\int_{\Gamma_S} (t_i - \tilde{t}_i) h_J(Q) d\Gamma - \int_{\Omega_S} \sigma_{ij,j} h_J(Q) d\Omega = 0 \tag{21}$$

$$\int_{\Gamma_S} (u_i - \tilde{u}_i) h_J(Q) d\Gamma = 0 \tag{22}$$

Based on hybrid displacement variational theory, the domain variables $\mathbf{u}$ and $\mathbf{t}$ are interpolated by the fundamental solution, which is

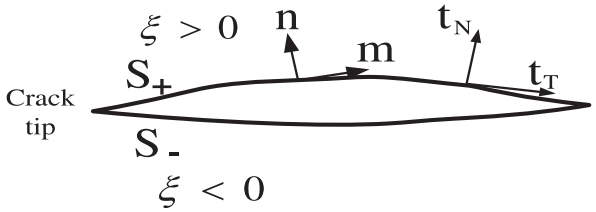

Fig. 2. Crack surface model.

$$\mathbf{u} = \begin{Bmatrix} u_1 \\ u_2 \end{Bmatrix} = \sum_{I=1}^{N_t} \begin{bmatrix} u_{11}^I & u_{12}^I \\ u_{21}^I & u_{22}^I \end{bmatrix} \begin{Bmatrix} x_1^I \\ x_2^I \end{Bmatrix} \tag{23}$$

$$\mathbf{t} = \begin{Bmatrix} t_1 \\ t_2 \end{Bmatrix} = \sum_{I=1}^{N_t} \begin{bmatrix} t_{11}^I & t_{12}^I \\ t_{21}^I & t_{22}^I \end{bmatrix} \begin{Bmatrix} x_1^I \\ x_2^I \end{Bmatrix} \tag{24}$$

where x_i^I is the unknown parameter, N_t is the total boundary node number, u_{ij}^I and t_{ij}^I are the fundamental solution with the source point of P^I (Fig. 1), which can be seen in references [42,43].

Substituting Eqs. (9), (13), (23) and (24) into Eqs. (21) and (22), the linear system equation can be rewritten as [42]

$$\sum_{I=1}^{N_t} \int_{\Gamma_S} \begin{bmatrix} t_{11}^I & t_{12}^I \\ t_{21}^I & t_{22}^I \end{bmatrix} \begin{Bmatrix} x_1^I \\ x_2^I \end{Bmatrix} h_J(Q) d\Gamma = \sum_{I=1}^{N_t} \int_{\Gamma_S} \begin{bmatrix} \Phi_I^t(s) & 0 & \Phi_I^t(s)H(\xi) & 0 \\ 0 & \Phi_I^t(s) & 0 & \Phi_I^t(s)H(\xi) \end{bmatrix} \begin{Bmatrix} t_1^I \\ t_2^I \\ b_1^I \\ b_2^I \end{Bmatrix} h_J(Q) d\Gamma \tag{25}$$

$$\sum_{I=1}^{N_t} \int_{\Gamma_S} \begin{bmatrix} u_{11}^I & u_{12}^I \\ u_{21}^I & u_{22}^I \end{bmatrix} \begin{Bmatrix} x_1^I \\ x_2^I \end{Bmatrix} h_J(Q) d\Gamma = \sum_{I=1}^{N_t} \int_{\Gamma_S} \begin{bmatrix} \Phi_I^u(s) & 0 & \Phi_I^u(s)H(\xi) & 0 \\ 0 & \Phi_I^u(s) & 0 & \Phi_I^u(s)H(\xi) \end{bmatrix} \begin{Bmatrix} u_1^I \\ u_2^I \\ a_1^I \\ a_2^I \end{Bmatrix} h_J(Q) d\Gamma \tag{26}$$

in which $\Phi_I^u(s)$, $\Phi_I^t(s)$ are shape functions for displacement and boundary traction of the present method, and a_1^I, b_1^I are additional node freedoms for discontinuity.

The system equations can be rewritten in matrix form, which is

$$\mathbf{Tx} = \mathbf{H}_t\mathbf{t} + \mathbf{C}_t\mathbf{b} \tag{27}$$

$$\mathbf{Ux} = \mathbf{H}_u\mathbf{u} + \mathbf{C}_u\mathbf{a} \tag{28}$$

in which **T, H, U** can be referred in [42,43], and **t, u** are boundary variable values, and

$$C_t^{IJ} = \int_{\Gamma_S} \Phi_I^t(s)H(\xi)h_J(Q)d\Gamma \tag{29}$$

$$C_u^{IJ} = \int_{\Gamma_S} \Phi_I^u(s)H(\xi)h_J(Q)d\Gamma \tag{30}$$

3. Frictional contact theory for HBNM

3.1. Contact model for HBNM

Consider a discontinuous surface S, which is shown in Fig. 2, and the discontinuity S includes two separate surfaces S_+ and S_-. According to contact theory, when the surfaces S_+ and S_- are closed under the compression, a normal traction and a tangential friction force arise.

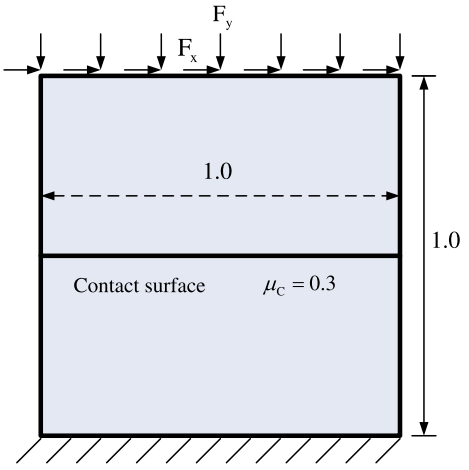

Fig. 3. Model of two sliding elastic bodies.

Based on Coulomb friction model, the normal gap function of discontinuous surface is given as [44,45]

$$g_N = [\mathbf{u}_{S+} - \mathbf{u}_{S-}] \cdot \mathbf{n} = \Delta\mathbf{u} \cdot \mathbf{n} \tag{31}$$

where $\mathbf{u}_{S+}$ and $\mathbf{u}_{S-}$ are the displacements at calculating node interpreted to lie on the S_+ and S_- sides of discontinuous surface S, respectively, and $\mathbf{n}$ is normal vector. And the relative tangential displacement vector can be given as

$$g_T = [\mathbf{u}_{S+} - \mathbf{u}_{S-}] \cdot \mathbf{m} = \Delta\mathbf{u} \cdot \mathbf{m} \tag{32}$$

in which $\mathbf{m}$ is tangential vector of discontinuous surface of calculating node.

In the present method, the constraint is handled by the penalty method, which can be given as

$$t_N = \varepsilon_N g_N \tag{33}$$

in which ε_N is the normal penalty parameter analogous to a normal spring that allows the contact surfaces to slightly overlap, and t_N is the normal component of traction on contact surface. And Coulomb friction model is employed in this paper, then

$$F_c(t_N, t_T) = \|t_T\| - \mu_C(t_N)\|t_N\| \begin{cases} = 0 & \text{slip} \\ < 0 & \text{stick} \end{cases} \tag{34}$$

in which t_T is the tangential component of traction on contact surface, and $\mu_C(t_N)$ is the frictional coefficient of contact surface. Then the traction vector $\mathbf{t}$ on discontinuous surface can be written as

$$\mathbf{t} = \begin{bmatrix} t_T \\ t_N \end{bmatrix} = \begin{bmatrix} G_T & 0 \\ 0 & \varepsilon_N \end{bmatrix} \begin{bmatrix} g_T \\ g_N \end{bmatrix} \tag{35}$$

in which G_T is tangential stiffness of contact surface.

In the normal direction, contact condition on the discontinuous surface S must be satisfied the constraint, which is

$$g_N \geq 0, \qquad t_N \leq 0, \qquad g_N t_N = 0 \tag{36}$$

The same as Eq. (36), a predictor–corrector scheme is constructed to obtain the tangential traction. So the traction predictor is

$$t_T^{\mathbf{tr}} = (t_T)_n + G_T \Delta g_T \tag{37}$$

in which $t_T^{\mathbf{tr}}$ is predicted value of tangential traction on contact surface, and $(t_T)_n$ is the tangential traction after n steps of iteration. Check whether $\|t_T^{\mathbf{tr}}\| + \mu_C \varepsilon_N g_N \leq 0$, if so, we accept the predictor as the final value, in which contact condition is stick; otherwise, we use the backward implicit algorithm to correct for plastic sliding, in which the contact condition is slip. So we can get the tangential traction by a

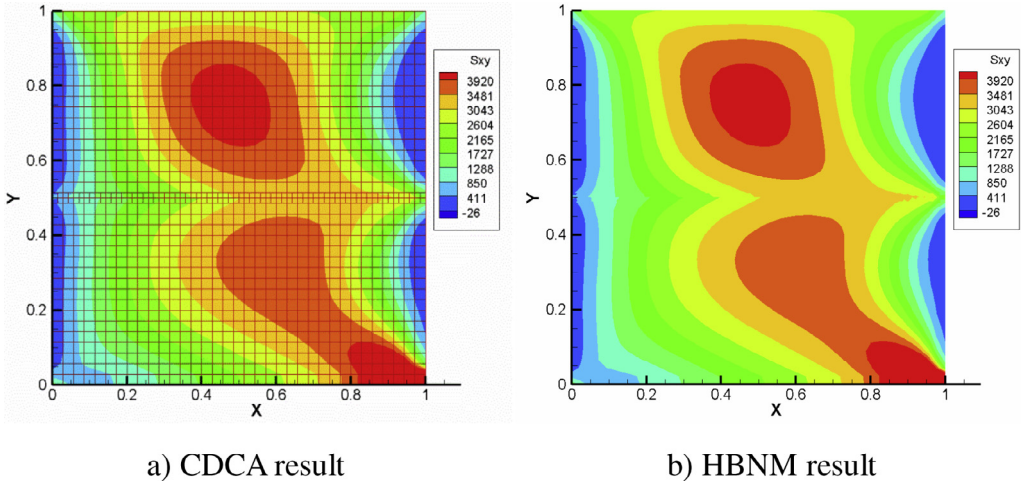

Fig. 4. Shear stress contours by different methods.

return mapping algorithm, which are

$$\begin{cases} (t_T)_{n+1} = (t_T)_n + G_T \Delta g_T & \left\| t_T^{\mathbf{tr}} \right\| + \mu_C \varepsilon_N g_N \le 0 \\ (t_T)_{n+1} = -\mu_C \varepsilon_N g_N \dfrac{t_T^{\mathbf{tr}}}{\left\| t_T^{\mathbf{tr}} \right\|} & \left\| t_T^{\mathbf{tr}} \right\| + \mu_C \varepsilon_N g_N > 0 \end{cases} \tag{38}$$

The iteration finishes when unbalanced force is equal to zero.

3.2. Additional equations

When discontinuous surface is close, a traction arises on discontinuous surface, and only Eqs. (27) and (28) cannot obtain the finally solution of contact problem, then several additional equation must be constructed. First, the traction on close contact surface must satisfy

$$t_T^{S+} + t_T^{S-} = 0 \tag{39}$$

$$t_N^{S+} + t_N^{S-} = 0 \tag{40}$$

As we know, Eqs. (39) and (40) must be satisfied on any location on contact surface, then, it must be satisfied on any integral subdomain Γ_s, then Eqs. (39) and (40) can rewritten as integral form, which is

$$\int_{\Gamma_S} t_T^{S+} d\Gamma + \int_{\Gamma_S} t_T^{S-} d\Gamma = 0 \tag{41}$$

$$\int_{\Gamma_S} t_N^{S+} d\Gamma + \int_{\Gamma_S} t_N^{S-} d\Gamma = 0 \tag{42}$$

Besides, a relation between crack opening displacement and contact stress can be constructed, based on Eq. (35), one can get

$$\mathbf{t} = \begin{bmatrix} t_T \\ t_N \end{bmatrix} = \begin{bmatrix} G_T & 0 \\ 0 & \varepsilon_N \end{bmatrix} \begin{bmatrix} g_T \\ g_N \end{bmatrix} = \mathbf{G}\Delta\mathbf{u} \tag{43}$$

in which $\mathbf{G}$ is the stiffness matrix related to normal and tangential contact stiffness, and $\Delta\mathbf{u}$ is a vector of crack opening displacement.

Combining Eqs. (27), (28), (41)–(43), one can get the solution of any contact problems.

4. Numerical examples

In order to illustrate the accuracy and efficiency of the present method in frictional contact problems, several numerical examples about fictional contact problems are given. After optimization, the radius of the sub-domain r_J is chosen as $0.8h$, with h being the average distance of the adjacent nodes, and $r_J/c_J = 1.25$ is applied.

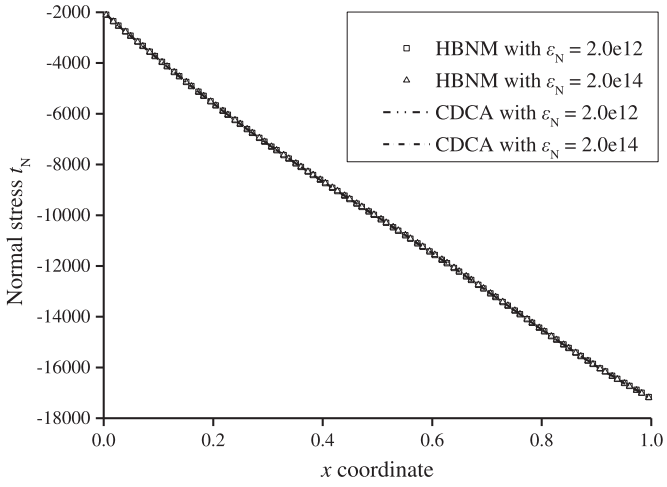

Fig. 5. Normal stress t_N by different methods.

4.1. Contact frictional behavior of two elastic bodies

Contact frictional behavior of two elastic bodies is considered in this section, and the model can be seen in Fig. 3 [44]. The bottom body is constrained at the bottom side, while a uniform horizontal and vertical loadings of $F_x = 2.5\times10^3$N/m and $F_y = 1.0\times10^4$ N/m are imposed on the top side of upper body. And the Young's modulus and Poisson's coefficient are given as: $E = 2.0\times10^{10}$ Pa and $\nu = 0.3$. The fictional coefficient between those two elastic bodies is $\mu_C = 0.3$.

In Fig. 4(a) and (b), the distribution of shear stress contours of τ_{xy} by different methods are presented, and it can be seen that the results by the present method are very close to those by continuous–discontinuous cellular automaton method (CDCA) [44].

Besides, the normal compressive stress and tangential fiction with different coordinates are shown in Figs. 5 and 6, in which one can see that those results by different methods greatly agree with each other. And it can be seen that normal stress is also no relation with the normal penalty parameter, but in order to ensure much little embedded displacement, ε_N should be much larger than Young's modulus. While the tangential stress is greatly influenced by the tangential stiffness of contact surface, and when $G_T = 1.0\times10^8$, it is shown that $x \le 0.56$, sliding occurs, but $x > 0.56$, two elastic block are stick, no relative sliding occurs, but $G_T = 1.0\times10^{10}$, it is shown that $x \le 0.65$, sliding occurs, but $x > 0.65$, two elastic block are stick.

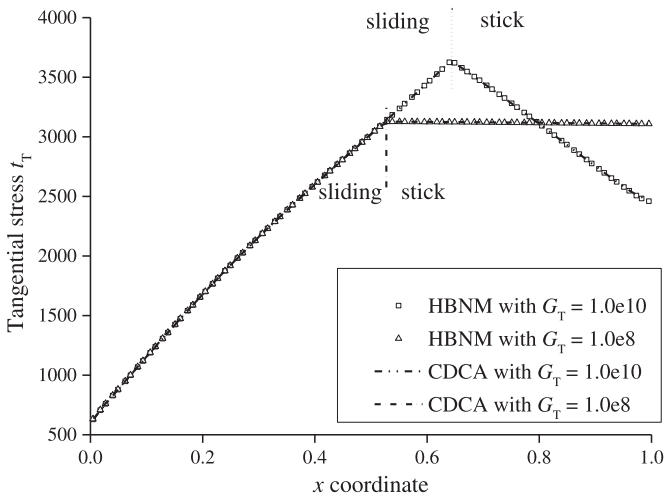

Fig. 6. Tangential stress t_T by different methods.

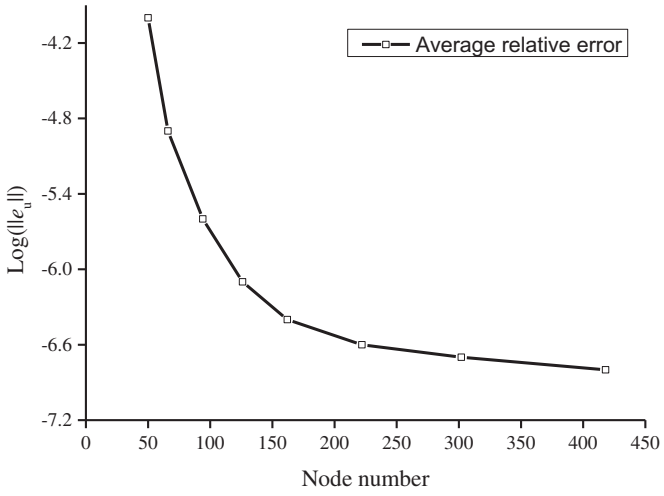

Fig. 7. Convergence of the present method.

Table 1
Normal stress t_N by different methods.

x coordinate	HBNM		CDCA	
	ϵ_N 2.0×10^{12}	ϵ_N 2.0×10^{14}	ϵ_N 2.0×10^{12}	ϵ_N 2.0×10^{14}
0.1	−3844.66	−3852.42	−3845.04	−3853.09
0.3	−7198.63	−7197.11	−7198.56	−7197.03
0.5	−10,076.01	−10,066.05	−10,076.29	−10,066.36
0.7	−12,987.35	−12,980.10	−12,988.00	−12,980.80
0.9	−15,948.30	−15,958.65	−15,947.39	−15,957.51

Table 2
Tangential stress t_T by different methods.

x coordinate	HBNM		CDCA	
	G_T 1.0×10^{8}	G_T 1.0×10^{10}	G_T 1.0×10^{8}	G_T 1.0×10^{10}
0.1	1155.73	1153.4	1156.08	1153.8
0.3	2159.14	2159.59	2159.10	2159.57
0.5	3019.81	3022.81	3019.90	3022.89
0.7	3121.45	3452.66	3121.49	3451.98
0.9	3112.49	2753.21	3112.56	2753.41

Normal stress and tangential stress on some nodes are given in Tables 1 and 2, in which a great agreement can be achieved between the present method results and CDCA results.

Fig. 7 plots the convergence curve of the present method, in which one can see that the present method converges quickly and smoothly, and the average relative error $e_u = \frac{1}{N}\sum_{i=1}^{N}|\frac{u_i - u_{\mathrm{CDCA}}}{u_{\mathrm{CDCA}}}|$, in which u_{CDCA} is the result by CDCA method [44] with 40,000 elements.

4.2. Compressive crack

A rectangle rock specimen with a compressive crack is considered in this section, the geometry of model and crack can be seen in Fig. 8, and the crack is located in the center of the rock specimen. Young's modulus of this specimen is $E = 5.0$ GPa, and Poisson's ratio is $\nu = 0.25$. Normal stiffness and tangential stiffness of crack surface are given as 1000 GPa and 10 GPa, and the coefficient of friction of crack surface is given as $\mu_c = 0.30$. The compressive stress is given as $F_y = 2.0$ MPa.

It can be seen in Figs. 9 and 10 that the normal stress t_N and tangential stress t_T are plotted, in which one can see that contact stress and friction on contact surface are agreed with each other by those two

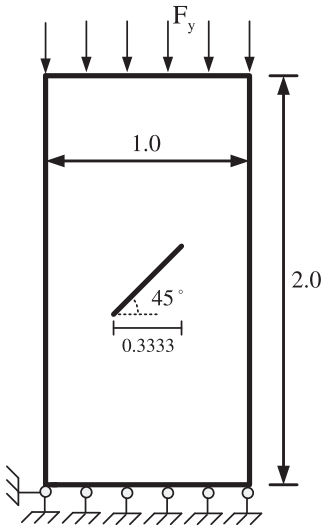

Fig. 8. Geometry and model of compressive crack.

methods, and the present method results is much more smooth than that by CDCA. It can be also seen that the tangential stiffness is no influenced to the contact stress in the present example, and results by different tangential stiffness are almost the same with each other.

4.3. Pull out of pile

A pile foundation simulation is considered in this section, and geometry of pile and soil model can be seen in Fig. 11, a half of model is considered for simplification. The material properties of the concrete pile are given as: $E_c = 2.0\times10^9$ Pa, $\nu_c = 0.3$ and density $\rho_c = 2.5\times10^3$ kg/m^3. The material properties of clay soil can be seen as: $E_s = 2.0\times10^8$, $\nu_c = 0.25$ and density $\rho_c = 2.0\times10^3$ kg/m^3. The contact friction behavior between pile and soil is modeled by the Mohr–Coulomb law with $c_f = 5.0$ kPa, $\mu_c = 0.58$ and the maximum tensile stress of $\sigma_s = 300$ kPa. The soil is restrained at the bottom and right hand edges, and a tensile force of $F_y = 50$ kN/m is imposed on the upper nodes of the pile. For comparison, results by continuous discontinuous cellular automaton method and XFEM are employed [44].

The shear stress on the contact surface of pile due to the pull-out force is presented in Fig. 12, in which the results obtained by Lei [46] and Liu and Borja [47] using extended finite element method (XFEM) and Yan et al. [44] using CDCA are employed for comparison. It can be seen that a great agreement can be achieved between those

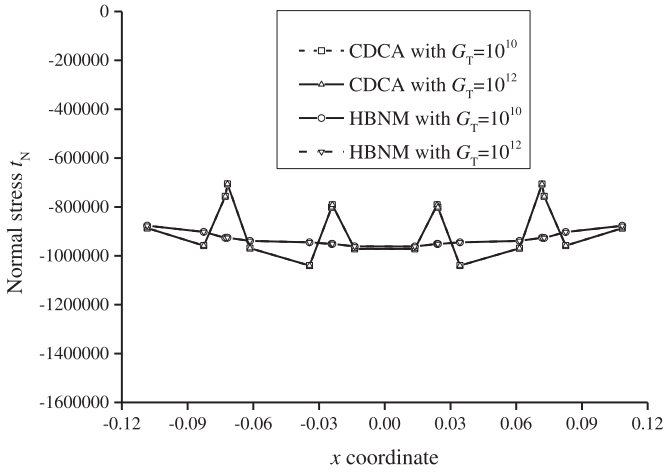

Fig. 9. Normal stress t_N by different methods.

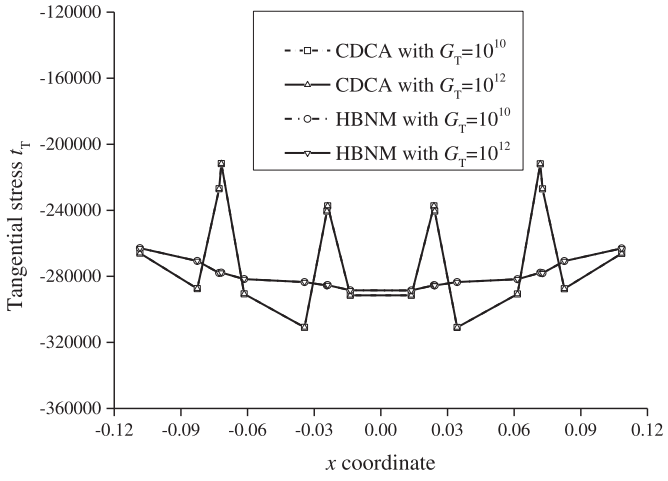

Fig. 10. Tangential stress t_T by different methods.

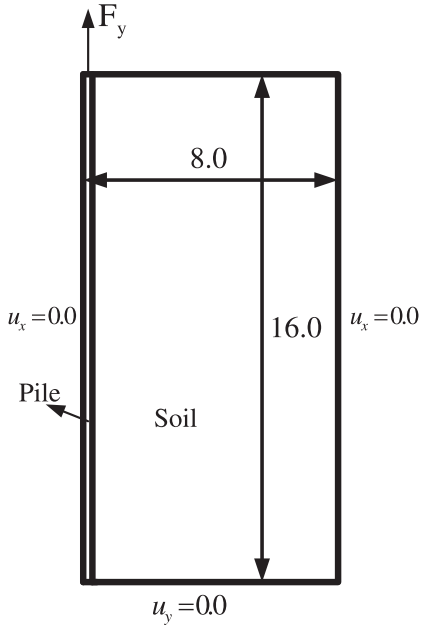

Fig. 11. Geometry and model of pile and soil structure.

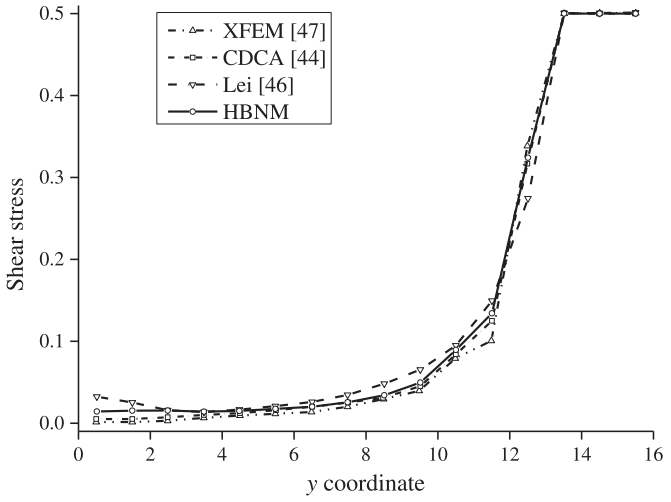

Fig. 12. Shear stress of contact surface between soil and pile.

four methods, which illustrates that the present method is effective and accurate.

5. Conclusions

In this paper, a continuous–discontinuous hybrid boundary node method for frictional contact problems is presented, in which the outer and internal boundaries are divided into several individual segments, for continuous segments on outer boundary, the radial point interpolation method is employed for shape function construction, for discontinuous segments, the enriched discontinuous basis functions combined with RPIM are developed, different from outer continuous segments, basis functions for displacement and traction are different and exactly reflect the properties of local displacement and stress around the crack tip, then the shape functions for displacement and traction on discontinuous surfaces are constructed individually. And the near tip asymptotic field functions and Heaviside function are employed for simulating the high gradient of stress field and discontinuous displacement field on contact surfaces.

Besides a frictional contact theory and complementation detail for hybrid boundary node method is proposed, and based on frictional contact theory, some additional equations are developed for frictional contact iteration. Based on above technique and theory, a continuous–discontinuous hybrid boundary node method is proposed for frictional contact problems. For comparison, some numerical results by the present method, CDCA and XFEM are given to illustrate that the present method is effective and accurate, and it can be widely used for some frictional contact engineering.

Acknowledgments

The work was financially supported by the National Natural Science Foundation of China (nos. 11232014, 51621006), the State Key Research Development Program of China (no. 2016YFC0600702), the International Partnership Program of Chinese Academy of Sciences (115242KYSB20160017), and Youth Innovation Promotion Association CAS (no. 2014304).

References

[1] Peric D, Owen DRJ. Computational model for contact problems with friction based on the penalty method. Int J Numer Methods Eng 1992;35:1289–309.
[2] Hildi P, Laborde P. Quadratic finite element methods for unilateral contact problems. Appl Numer Math 2002;41:401–21.
[3] Kikuchi N, Oden JT. Contact problems in elasticity: a study of variational inequalities and finite element methods. Philadelphia: SIAM; 1988.

[4] Hughes TJR, Taylor RL, Sackman JL, Curnier A, Kanoknukulchai W. A finite element method for a class of contact-impact problems. Comput Methods Appl Mech Eng 1976;8:249–76.
[5] Xiao HT, Yue ZQ. A generalized Kelvin solution based BEM for contact problems of elastic indenter on functionally graded materials. Comput Modell Eng Sci 2009;52:159–79.
[6] Gun H, Gao XW. Analysis of frictional contact problems for functionally graded materials using BEM. Eng Anal Bound Elem 2014;38:1–7.
[7] Olukoko OA, Becker AA, Fenner RT. A review of three alternative approaches to modeling frictional contact problems using the boundary element method. Proc R Soc A 1994;444:37–51.
[8] Hack RS, Becker AA. Frictional contact analysis under tangential loading using a local axes boundary element formulation. Int J Mech Sci 1999;41:419–36.
[9] Gun H. Boundary element analysis of 3D elasto-plastic contact problems with friction. Comput Struct 2004;82:555–66.
[10] Li Q, Lee KM. An adaptive meshless method for analyzing large mechanical deformation and contacts. J Appl Mech 2008;75:041014 Trans ASME.
[11] Belaasilia Y, Timesli A, Braikat B, Jamal M. A numerical meshfree model for elasto–plastic contact problems. Eng Anal Bound Elem 2017;82:68–78.
[12] Gun H. Isotropic damage analysis of frictional contact problems using quadratic meshless boundary element method. Int J Mech Sci 2014;80:102–8.
[13] Hu DA, Long SY, Han X, Li GY. A meshless local Petrov-Galerkin method for large deformation contact analysis of elastomers. Eng Anal Bound Elem 2007;31:657–66.
[14] Xiao JR, Gama BA, Gillespie JW Jr, Kansa EJ. Meshless solutions of 2D contact problems by subdomain variational inequality and MLPG method with radial basis functions. Eng Anal Bound Elem 2005;29:95–106.
[15] Li D, Bai B, Cheng Y, Liew KM. A novel complex variable element free Galerkin method for two-dimensional large deformation problems. Comput Methods Appl Mech Eng 2012;233–236:1–10.
[16] Timesli A, Braikat B, Zahrouni H, Moufki A, Lahmam H. An implicit algorithm based on continuous moving least square to simulate material mixing in friction stir welding process. Modell Simul Eng 2013;2013:1–14.
[17] Timesli A, Braikat B, Lahmam H, Zahrouni H. A new algorithm based on moving least square method to simulate material mixing in friction stir welding. Eng Anal Bound Elem 2015;50:372–80.
[18] Mesmoudi S., Timesli A., Braikat B., Lahmam H., Zahrouni H. A 2d mechanical-thermal coupled model to simulate material mixing observed in friction stir welding process. Eng Comput 2017:1–11
[19] Belytschko T, Fleming M. Smoothing, enrichment and contact in the element-free Galerkin method. Comput Struct 1999;71:173–95.
[20] Tiago C, Pimenta PM. An EFG method for the nonlinear analysis of plates undergoing arbitrarily large deformations. Eng Anal Bound Elem 2008;32(6):494–511.
[21] Ullah Z, Augarde CE. Finite deformation elasto-plastic modeling using an adaptive meshless method. Comput Struct 2013;118:39–52.
[22] Guedes CF, Cesarde Sa JMA. A proposal to deal with contact and friction by blending meshfree and finite element methods in forming processes. Int J Mater Form 2008;1:177–88.
[23] Youssef B, et al. A numerical mesh-free model for elasto-plastic contact problems. Eng Anal Bound Elem 2017;82:68–78.
[24] Chen JS, Wang HP, Yoon S, You Y. Some recent improvements in meshfree methods for incompressible finite elasticity boundary value problems with contact. Comput Mech 2000;25(2–3):137–56.
[25] Campbell J, Vignjevic R, Libersky L. A contact algorithm for smoothed particle hydrodynamics. Comput Methods Appl Mech Eng 2000;184:49–65.
[26] Attaway SW, Heinstein MW, Swegle JW. Coupling of smooth particle hydrodynamics with the finite element method. Nucl Eng Design 1994;150:199–205.
[27] Kulasegaram S, Bonet J, Lewis RW, Profit M. A variational formulation based contact algorithm for rigid boundaries in two-dimensional SPH applications. Comput Mech 2004;33:316–25.
[28] Kim NH, Choi KK, Chen JS, Park YH. Meshless shape design sensitivity analysis and optimization for contact problem with friction. Comput Mech 2000;25:157–68.
[29] Chen JS, Pan C, Button ST. Analysis of metal forming process based on meshless method. J Mater Process Technol 1998;80–81:642–6.
[30] Li Y, et al. Contact analysis for solids based on linearly conforming radial point interpolation method. Comput Mech 2007;39:537–54.
[31] Zheng G, Cui X, Li G, Wu S. A linearly conforming radial point interpolation method (LC-RPIM) for contact problems in metal forming analysis. Int J Mater Form 2010;3(1):891–4.
[32] Chen JS, Wang HP. New boundary condition treatments for meshless computation of contact problems. Comput Methods Appl Mech Eng 2001;187(3–4):441–68.
[33] Zhang JM, Yao ZH, Li H. A Hybrid boundary node method. Int J Numer Methods Eng 2002;53:751–63.
[34] Mukherjee YX, Mukherjee S. The boundary node method for potential problems. Int J Numer Methods Eng 1997;40:797–815.
[35] Miao Y, Wang YH, Yu F. An improved hybrid boundary node method in two-dimensional solids. Acta Mech Solida Sin 2005;18:307–15.
[36] Nardini D, Brebbia CA. Transient dynamic analysis by the boundary element method. Boundary element methods in engineering. Southampton/Berlin and New York: Computational Mechanics Publications/Springer; 1983.
[37] Yan F, Wang YH, Tham LG, Cheung YK. Dual reciprocity hybrid boundary node method for 2-D elasticity with body force. Eng Anal Bound Elem 2008;32:713–25.
[38] Yan F, Wang YH, Miao Y, Tham LG, Cheung YK. Dual reciprocity hybrid boundary node method for free vibration analysis. J Sound Vib 2009;321(3–5):1036–57.
[39] Yan F, Miao Y, Yang QN. Quasilinear hybrid boundary node method for solving nonlinear problems. Comput Model Eng Sci 2009;46(1):21–50.
[40] Yan F, Yu M, Lv JH. Dual reciprocity boundary node method for convection-diffusion problems. Eng Anal Bound Elem 2017;80:230–6.
[41] Yan F, Feng XT, Lv JH, Pan PZ. A new hybrid boundary node method based on Taylor expansion and Shepard interpolation method. Int J Numer Methods Eng 2015;102:1488–506.
[42] Yan F, Feng XT, Lv JH, Li SJ. The continuous-discontinuous hybrid boundary node method for solving stress intensity factor. Eng Anal Bound Elem 2017;81:35–43.
[43] Yan F, Feng XT, Zhou H. A dual reciprocity hybrid radial boundary node method based on radial point interpolation method. Comput Mech 2010;45:541–52.
[44] Yan F, Feng XT, Pan PZ, Li YP. A continuous- discontinuous cellular automaton method for regular frictional contact problems. Arch Appl Mech 2013;83(8):1239–55.
[45] Yan F, Feng XT, Pan PZ, Li SJ. Rock initiation and propagation simulation under compression-shear loading using continuous-discontinuous cellular automaton method. Acta Mech Solida Sin 2015;28(4):384–99.
[46] Lei XY. Contact friction analysis with a simple interface element. Comput Methods Appl Mech Eng 2001;190:1955–65.
[47] Liu FS, Borja RI. Stabilized low-order finite elements for frictional contact with the extended finite element method. Comput Methods Appl Mech Eng 2010;199:2456–71.